Journal of Materials and Environmental Sciences
ISSN : 2028-2508
CODEN : JMESCN

Copyright © 2018,
University of Mohammed Premier
Oujda Morocco

J. Mater. Environ. Sci., 2018, Volume 9, Issue 10, Page 2904-2912

http://www.jmaterenvironsci.com

Optical properties of desert aerosol –II–

J. Barkani[1], A. Tahiri[2], M. Diouri[2*]

[1] *Laboratory of Engineering Sciences (LSI), Polydisciplinary Faculty of Taza, University Sidi Mohamed Ben Abdellah, Fez, Morocco*

[2] *Atmospheric physics team (L.M.E), Faculty of science, University Mohamed First, Oujda, Morocco*

Received 01 Oct 2017,
Revised 08 Jun 2018,
Accepted 20 Jun 2018

Keywords

- ✓ *Desert Aerosol,*
- ✓ *Angstrom Exponent,*
- ✓ *Particle Size Distribution,*
- ✓ *Refractive Index,*
- ✓ *Asymmetry Factor.*

dyourim@gmail.com ;
Phone: (+212) 661298191

Abstract

The optical parameters of the desert aerosol at six sites representative of the desert zones: Oujda and Ouarzazate (Morocco, North Africa), Tamanrasset (Algeria, North Africa), Birdsville (Australia), Dalanzadgad (Mongolia, Asia) and Frenchman-Flat (Nevada, West of United States) are determined. The particle size distributions is near 0.145 µm for the fine particles and 2.06 µm for the coarse ones. The largest volume concentration recorded at Tamanrasset (0.271$\mu m^3/\mu m^2$), due mainly to the coarse particles mode (0.255 $\mu m^3/\mu m^2$) in agreement with the Angstrom coefficients of the order of 0.2. Birdsville and Frenchman-Flat registred the lowest concentrations of the order of 0.030 $\mu m^3/\mu m^2$. The asymmetry factor has a high regularity around 0.65 for fine particles and 0.90 for coarse particles. The diversity of the desert origin shows some variation of the real part of the refractive index of 1.564 (Birdsville) at 1.643 (Frenchman-Flat) and the imaginary part of 13.10^{-3} (Tamanrasset) at 157.10^{-3} (Birdsville).

1. Introduction

Saharan mineral dust plays an important role in the climate system. They are essential for understanding the processes of formation, transport and modification of various desert air masses. They can travel thousands of kilometers away from the source. The interaction between mineral dust and solar radiation is complex. The minerals can be absorbers or diffusers of light according to their mineralogical composition and the wavelength. Aerosols of desert origin mainly lead to the cooling of the earth-atmosphere system [1]. Desert aerosols are composed of a mixture of various mineralogical compounds such as clays (Illite, kaolinite, and chlorite), feldspars, quartz, calcite and iron oxides (hematite, goethite) [2]. The estimation of their complex refractive indices is difficult because the chemical composition of the aerosols varies according to the soil, the multiple physical processes responsible for their uplift and the sources not activated constantly throughout the year. The variability and ignorance of the absorbent properties of these aerosols are still the main sources of uncertainty in the quantification of their radiative impacts. The spectral radiative behavior of the diffusion and absorption processes is based the complex refractive index, involving particle size distributions, chemical composition, source, particle mixing state and Shape of the particles.

A global network of sun-sky radiometers, Aerosol Robotic Network (AERONET/PHOTONS) established by the National Aeronautics and Space Administration (NASA, USA) and the Atmospheric Optics Laboratory (LOA, CNRS France). The network enhanced by various collaborations of national agencies, institutes, universities including Mohamed Premier University (Faculty of Sciences Oujda since 2010), scientists and associates around the world. The purpose of the AERONET network is to characterize the properties of aerosols by constituting a continuous and useful database, particularly for aerosol climatology, to validate the data obtained from satellite observations. It produces data on the properties of aerosols which are the optical thickness of AOT aerosols; The Angstrom exponent; Size distribution; The single scattering albedo; The asymmetry factor; The refractive index; The phase function; Radiative forcing based on the measurements of

the spectral extinction of the directly transmitted solar radiation and the inversion products [3]. The AOT parameter, obtained from the directly transmitted irradiance data measured by the CIMEL solar photometers of the AERONET network, is an indicator of the quantities of aerosols in the vertical column of the atmosphere and constitutes the main parameter for evaluating the radiative forcing [1]. The Angstrom exponent, determined from the spectral dependence of AOT, is an indicator of particle size and its variations [4].

The real part of the refractive index of desert aerosols determines the size of the diffusion and varies in the interval (1.51, 1.56) [5-7]. The imaginary part defines the absorbing power and is estimated between 3.1 10^{-3} and 5.2 10^{-3} for the wavelength 0.45 μm and varies from 0.310^{-3} to 2.510^{-3} for 0.70 μm [6].

In this paper, we study Angstrom Exponent, Volume distribution of the aerosol, Asymmetry factor and refractive index for Ouarzazate, Oujda (Morocco, North Africa), Tamanrasset (Algeria, North Africa), Dalanzadgad (Mongolia, Asia), Birdsville (Australia) and Frenchman-Flat (Nevada, USA).

2. Angstrom Exponent

The solar photometric measurements of the optical thickness of the AOT aerosols determine the atmospheric turbidity coefficient β and the Angstrom Exponent α (or aerosol size coefficient) from the Angstrom formula [8]:

$$\tau_a(\lambda) = \beta\lambda^{-\alpha} \qquad (1)$$

Where $\tau_a(\lambda)$ is the optical thickness of the wavelength. Thus, the expression of the Angstrom exponent α is established by eliminating the coefficient β for two optical thicknesses $\tau_a(\lambda_1)$ and $\tau_a(\lambda_2)$ at the respective wavelengths λ_1 and λ_2 and is written:

$$\alpha_{1-2} = -\frac{\ln\frac{\tau_a(\lambda_1)}{\tau_a(\lambda_2)}}{\ln\frac{\lambda_1}{\lambda_2}} \qquad (2)$$

To determine the optical thickness of the aerosol (AOT) at the wavelength λ = 0.5 μm, the AOT values at λ = 0.44 μm and at λ = 0.87μm, are used in the Angstrom formula and considering the Angstrom exponent α unique in the 0.44-0.87 μm spectral band. The choice of wavelength λ = 0.5 μm has been widely used in numerous studies of atmospheric aerosols, Holben et al. [2001] [9], El Amraoui and Diouri [10], [11] and A. Tahiri [2015] [12].

In Oujda (Fig. 1.a) the values of the Angstrom Exponent show two minimum peaks during spring and summer with values less than 0.5 seasons for which the aerosol is dominated by the large particles of Saharan origin coming mainly from the South-East of Morocco. The maximum value near 2.0 observed in February. The large values observed in autumn and winter confirm the presence of fine particles. These results are in agreement with those observed in earlier studies [13; 14].

The annual cycle at Ouarzazate presented in Fig .1.b. The peak dust dominated seasons are spring and summer when average α < 0.6 (AOT > 0.4), while the highest monthly mean occurs in december at 1.6. The primary sources of aerosol in Ouarzazate are desert dust from the Sahara.

For the Tamanrasset site (Fig.1.c) the values of the daily averages are less than 0.22, they represent the high AOT values (≥ 0.3) during spring and summer, reflecting the presence of desert dust (Super-micron particles), is practically within the Saharan sources. For the autumn and winter, large values of α (≥ 0.18) with a maximum observed in February (0.86) and low AOT values (≤ 0.15) with a minimum value of 0.01 are observed. These values confirm that the aerosol may be dominate by submicron particles, due to the anthropogenic contribution of industrial zones in Libya and Algeria.

The Birdsville site (Fig.1.d) daily averages show an apparent seasonal cycle, as well as large variations in daily measurements, including negative values in some days, especially during the autumn, which is probably due to activity of dust storms. The large values of α (≥ 0.5) and the low AOT values suggest a contribution of different types of aerosols such as biomass burning and influence of marine emissions comes from the ocean.

The values observed at Dalanzadgad (Fig.1.e) are greater than 0.5 for all seasons in 2014, the maximum value is observed in June (~ 1.9) and the minimum value in November (~ 0.02). Because of its high altitude and its remoteness from any sea, Mongolia has an extreme continental climate: Fall, quickly frosty and it can snow in September. Winter is very cold (-30 °C) and there is little snow. Spring: season is experiencing sandstorms. The summer is short but hot, especially in the Gobi Desert.

For the Frenchman-Flat (Fig.1.f) site, the annual cycle varies in contrast to the AOT, and have values greater than 0.5. These show the influence of aerosols from flat sand and salt grounds (Table 1).

Table 1: Annual averages of Angstrom Exponent (0.44-0.87 µm)

Site	AE (0.44-0.87 µm)
Oujda 2015	0.82 ± 0.42
Ouarzazate 2015	0.43 ± 0.29
Tamanrasset 2015	0.29 ± 0.20
Birdsville 2015	0.79 ± 0.48
Dalanzadgad 2014	0.85 ± 0.39
Frenchman-Flat 2013	1.04 ± 0.36

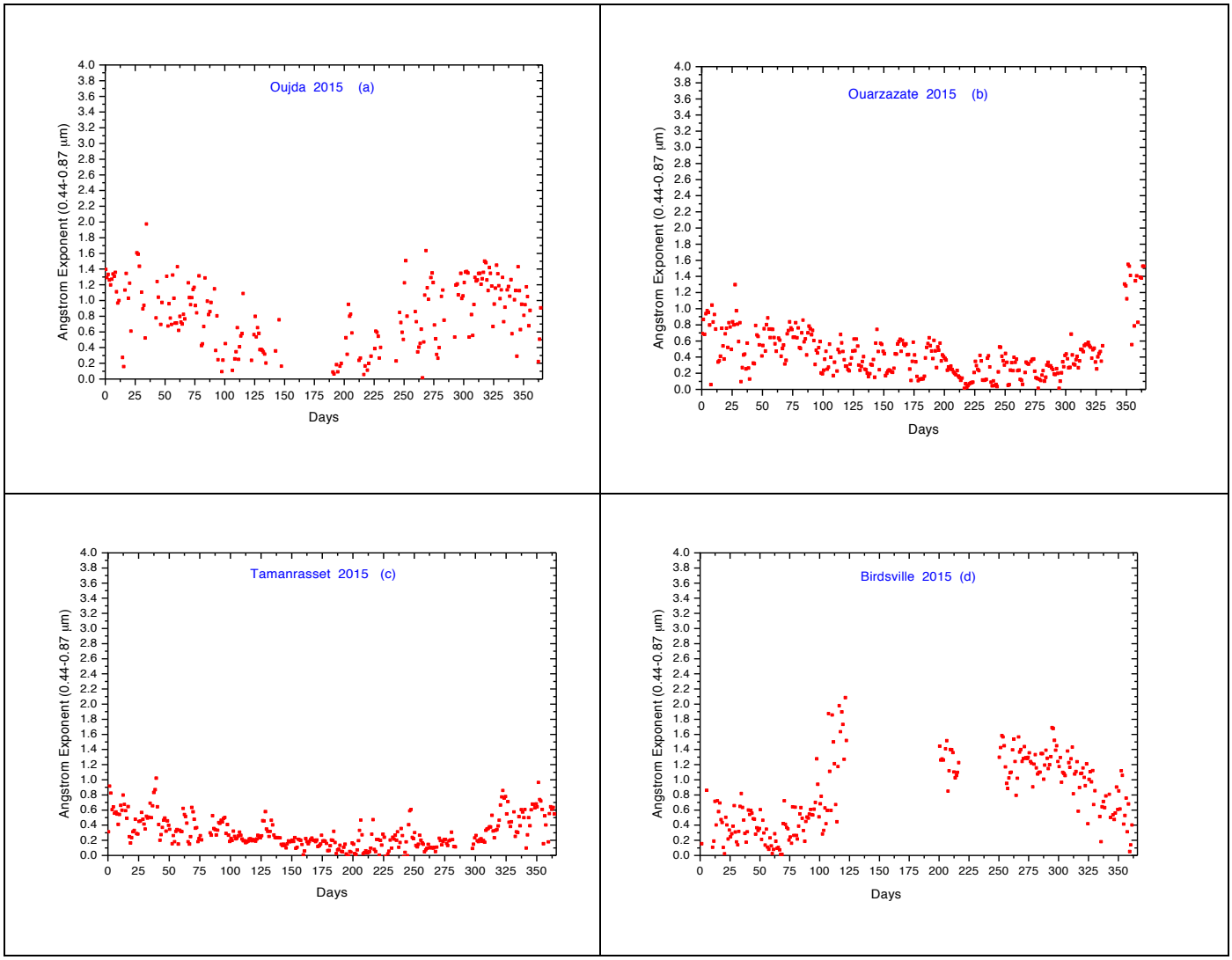

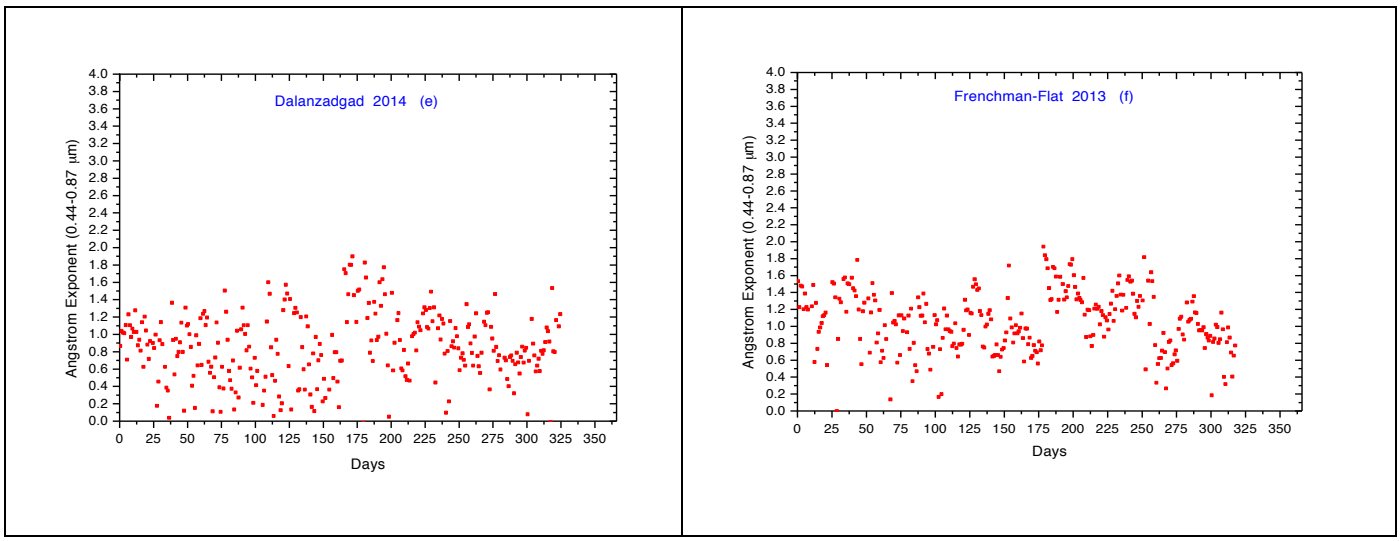

Figure 1: Daily averages of Angstrom Exponent (0.44-0.87 µm) of aerosols particle

3. Particle size distribution

The volume particle size distribution dV(r)/dlnr ($\mu m^3/\mu m^2$) is retrieved for 22 logarithmically equidistant discrete points (r_i) in the range of sizes 0.05µm ≤ r ≤ 15µm. The real n (λ) (1.33 ≤ n (λ) ≤1.6) and imaginary k (λ) parts of the complex refractive index (0.0005 ≤ k (λ) ≤ 0.5) are retrieved for the wavelengths corresponding to sky radiance measurements. The retrieval provides the percentage of spherical particles in the observed aerosol [15]. In addition to the detailed size distribution, the retrieval provides the following standard parameters for total (t), fine (f) and coarse (c) aerosol modes:

- ✓ Volume concentration ($\mu m^3/\mu m^2$) :

$$c_v = \int_{r_{\min}}^{r_{\max}} \frac{dV(\mathrm{r})}{d\ln r} d\ln r \qquad (3)$$

- ✓ Volume median radius (mean logarithm of radius):

$$\ln r_v = \frac{\int_{r_{\min}}^{r_{\max}} \ln r \frac{dV(\mathrm{r})}{d\ln r} d\ln r}{\int_{r_{\min}}^{r_{\max}} \frac{dV(\mathrm{r})}{d\ln r} d\ln r} \qquad (4)$$

- ✓ Standard deviation from volume median radius (mean logarithm of radius):

$$\sigma_v = \sqrt{\frac{\int_{r_{\min}}^{r_{\max}} (\ln r - \ln r_v)^2 \frac{dV(\mathrm{r})}{d\ln r} d\ln r}{\int_{r_{\min}}^{r_{\max}} \frac{dV(\mathrm{r})}{d\ln r} d\ln r}} \qquad (5)$$

- ✓ Effective radius :

$$r_{eff} = \frac{\int_{r_{\min}}^{r_{\max}} r^3 \frac{dN(\mathrm{r})}{d\ln r} d\ln r}{\int_{r_{\min}}^{r_{\max}} r^2 \frac{dN(\mathrm{r})}{d\ln r} d\ln r} \qquad (6)$$

The separation point between fine and coarse mode particles is near 0.44 µm. Using that separation, the code determine the size distribution data in two log-normal modes described by equation (7):

$$\frac{dV}{d\ln r} = \frac{C_f}{\sqrt{2\pi}\ln\sigma_f} \exp - \left(\frac{\left|\ln r - \ln r_{m_f}\right|^2}{2\left(\ln\sigma_f\right)^2} \right) + \frac{C_c}{\sqrt{2\pi}\ln\sigma_c} \exp - \left(\frac{\left|\ln r - \ln r_{m_c}\right|^2}{2\left(\ln\sigma_c\right)^2} \right) \qquad (7)$$

Where the C is total mode volume ($\mu m^3/\mu m^2$) and the subscripts f and c denote fine and coarse modes respectively. σ is the geometric standard deviation and r_{mf} (r_{mc}) is the geometric fine (coarse) mean radius.
We distinct two categories of distributions, distributions whose volume concentration of total mode exceeds 0.1 µm and distributions in the range (0.03, 0.059) µm. The first concerns the sites of Tamanrasset and Ouarzazate with high values of the coarse mode. Fine particles varies from 0.162 to 0.179 µm and coarses varies between 2.282 and 2.596 µm. The second covers the sites of Oujda, Birdsville, Dalanzadgad and Frenchman-Flat where fine mode ranging from 0.133 to 0.171µm and coarse mode ranging from 2.223 to 2.729 µm. The large annual mean values of the volume concentrations of coarse aerosol particles are observed for Ouarzazate (0.255 ± 0.321 $\mu m^3/\mu m^2$) and Tamanrasset (0.084 ± 0.160 $\mu m^3/\mu m^2$), since these regions have high atmospheric loads of desert dust. The detailed results of annual means characteristics given in table 2.

Table 2: Annual means characteristics of particle size distribution.

Site / Modes	Total	Fine particles	Coarse particles
Oujda			
c_v ($\mu m^3/\mu m^2$)	0.051 ± 0.081	0.011 ± 0.009	0.039 ± 0.077
r_v (µm)	1.198 ± 0.433	0.154 ± 0.032	2.638 ± 0.472
r_{eff} (µm)	0.466 ± 0.215	0.135 ± 0.020	2.107 ± 0.429
σ_v	1.366 ± 0.208	0.495 ± 0.059	0.689 ± 0.084
Ouarzazate			
c_v ($\mu m^3/\mu m^2$)	0.096 ± 0.167	0.111 ± 0.008	0.084 ± 0.160
r_v (µm)	1.436 ± 0.319	0.162 ± 0.024	2.596 ± 0.651
r_{eff} (µm)	1.254 ± 0.237	0.137 ± 0.018	2.044 ± 0.525
σ_v	0.588 ± 0.191	0.586 ± 0.064	0.672 ± 0.071
Tamanrasset			
c_v ($\mu m^3/\mu m^2$)	0.271 ± 0.332	0.016 ± 0.012	0.255 ± 0.321
r_v (µm)	1.770 ± 0.358	0.179 ± 0.045	2.282 ± 0.563
r_{eff} (µm)	0.924 ± 0.227	0.151 ± 0.039	1.889 ± 0.429
σ_v	0.937 ± 0.162	0.596 ± 0.083	0.588 ± 0.074
Birdsville			
c_v ($\mu m^3/\mu m^2$)	0.035 ± 0.054	0.006 ± 0.003	0.029 ± 0.053
r_v (µm)	1.477 ± 0.567	0.187 ± 0.033	2.869 ± 0.485
r_{eff} (µm)	1.323 ± 0.174	0.165 ± 0.026	2.162 ± 0.429
σ_v	0.602 ± 0.301	0.496 ± 0.046	0.731 ± 0.058
Dalanzadgad			
c_v ($\mu m^3/\mu m^2$)	0.059 ± 0.065	0.009 ± 0.006	0.049 ± 0.061
r_v (µm)	1.435 ± 0.474	0.157 ± 0.025	2.597 ± 0.503
r_{eff} (µm)	0.573 ± 0.223	0.139 ± 0.019	2.016 ± 0.381
σ_v	1.280 ± 0.174	0.494 ± 0.055	0.693 ± 0.055
Frenchman-Flat			
c_v ($\mu m^3/\mu m^2$)	0.030 ± 0.024	0.009 ± 0.010	0.021 ± 0.017
r_v (µm)	1.244 ± 0.550	0.164 ± 0.028	2.816 ± 0.612
r_{eff} (µm)	0.472 ± 0.216	0.147 ± 0.022	2.147 ± 0.473
σ_v	1.391 ± 0.156	0.467 ± 0.049	0.716 ± 0.068

4. Asymmetry factor

The asymmetry factor (g) defined as the average value of the cosine of the diffusion angle (θ) over the set of diffusion directions can be calculated from the phase function P (θ, λ) which represents the angular distribution of the scattered radiation at a given wavelength [16]:

$$g(\lambda) = \langle \cos\theta \rangle = \frac{1}{2}\int_0^{\pi} \cos(\theta).P(\theta,\lambda).\sin(\theta)d\theta \qquad (8)$$

For total backscattering at 180 °, g is -1, for isotropic diffusion, g is 0 and for total diffusion in the direction of the incident radiation, g is equal to 1.
The atmospheric aerosol, with a positive asymmetry factor means that most of the scattered radiation is forward. The larger the particle size, the more forward scattering (low scattering angle) and therefore the value of the asymmetry factor is closer to 1. For Oujda (Fig. 2.a), the daily averages of the asymmetry factors for large

particles vary between 0.75 and 0.96 with a significant change depending on days. The fine particles vary between 0.52 and 0.79.Ouarazazate (Fig. 2.b) shows a large variation with values between 0.48 and 0.75 for the coarse particles, while we observe a variation of 0.78 to 0.96 for the fine particles.

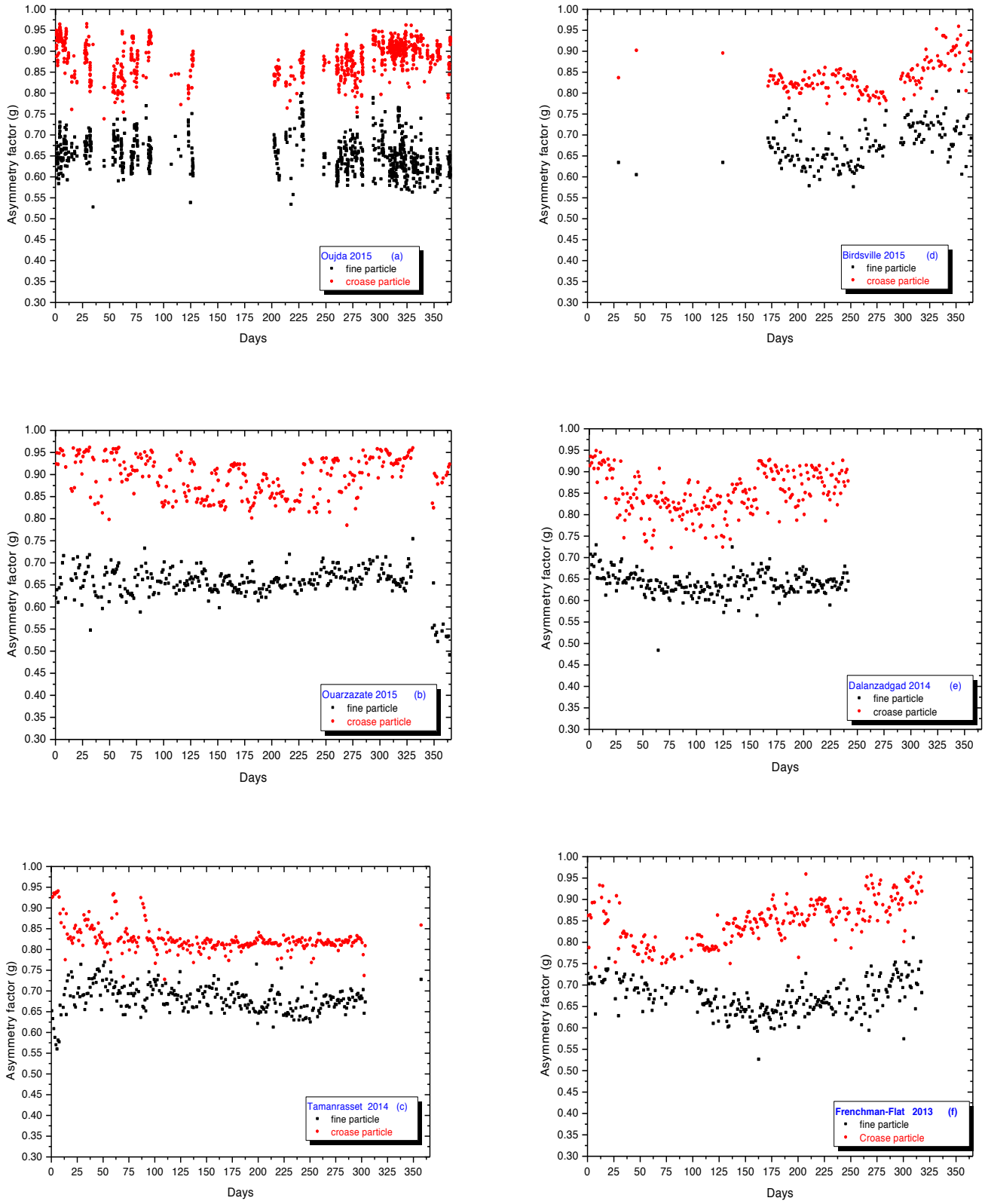

Figure 2: Daily means of asymmetry factor (0.44 µm) for aerosols particles for Oujda (a), Ouarzazate (b), Tamanrasset (c), Birdsville (d), Dalanzadgad (e) and Frenchman-Flat (f)

For Tamanrasset the variation between 0.57 and 0.80 (Fig. 2.c) observed for fine particles, whereas for large particles there is a variation of 0.77 to 0.96. For Birdsville, Dalanzadgad, and Frenchmen-Flat (Fig.2.d, e, f), a large variation of (g) for the wavelength 0.44 µm is observed with variations from 0.47 to 0.81 for the fine particles and between 0.72 and 0.96 for coarse particles. For the six sites, the asymmetry factors exhibit significant spatial and temporal variations, and vary between 0.72 and 0.96 for the coarse particles, thus showing a diffusion of the light especially towards the front. The annual mean values seems more constant close to 0.65 for fines particles and 0.84 for coarse, the detailed results of annual means are given in table 3.

Table 3: Annual means of asymmetry factor (total, fine, coarse) for 0.44 µm.

Site	Asymmetry factor (0.44 µm)		
	Total	Fine particle	Coarse particle
Oujda 2015	0.702 ± 0.041	0.651 ± 0.040	0.872 ± 0.039
Ouarzazate 2015	0.733 ± 0.039	0.654 ± 0.035	0.893 ± 0.044
Tamanrasset 2015	0.768 ± 0.023	0.680 ± 0.033	0.823 ± 0.032
Birdsville 2015	0.720 ± 0.042	0.672 ± 0.031	0.871 ± 0.048
Dalanzadgad 2014	0.696 ± 0.028	0.638 ± 0.027	0.848 ± 0.050
Frenchman-Flat 2013	0.707 ± 0.034	0.668 ± 0.039	0.849 ± 0.051

5. Complex refractive index

The complex refractive index m varies as a function of wavelength and is determined for wavelengths ranging from Ultra-Violet to Near Infra-Red (0.44 - 0.675 - 0.87 - 1.02 µm). It depends on the constituents, so it can be very different from one aerosol to another. This index is a complex number, the real part indicated the ability of the particle to diffuse (1.33 to 1.6) and the imaginary part its capacity to absorb (0.0005 to 0.5), m is defined by the following complex representation:

$$m(\lambda) = n_{re}(\lambda) - ik_{im}(\lambda) \qquad (9)$$

The refractive index is an important parameter in the estimation of direct radiative forcing of aerosols. Several authors [17, 18, 19] propose very different estimates in particular with respect to the imaginary part varying between 810^{-3} and 1010^{-3} to 0.50 µm. With the latest measurement campaigns (SHADE, DABEX, DODO, SAMUM), more accurate estimates of the refractive index of Saharan aerosols (Table 4) were obtained.

Table 4: Annual means of the real and imaginary part (0.44µm) for refractive index of desert aerosol

Localization	$\lambda_{0.40\ ;\ 0.45}$ µm	$\lambda_{0.65\ ;\ 0.70}$ µm	References
Mesures au sol Tinfou (Maroc)	$1.530 - 05.110^{-3}$ i	$1.530 - 0.4510^{-3}$ i	Müller et al, 2009 [20]
Mesures au sol Tinfou (Maroc)	$1.570 - 06.610^{-3}$ i	$1.550 - 0.3310^{-3}$ i	Kandler et al, 2009 [2]
Mesures au sol Cap Vert	$1.575 - 12.010^{-3}$ i	$1.573 - 0.6710^{-3}$ i	Kandler et al, 2011 [21]
Mesures avion région Cap Vert	$1.550 - 04.010^{-3}$ i	$1.546 - 1.0010^{-3}$ i	Weinzierl et al, 2011 [22]

In table 5, the annual averages of the values of the real part and the imaginary part of the refractive index for the six sites are given respectively. For Ouarzazate, Birdsville and Dalanzadgad, the real part vary between 1.510 ± 0.053and 1.564 ± 0.037 for the 0.44 µm wavelength. The sites of Oujda, Tamanrasset and Frenchman-Flat have values ranging between 1.483 ± 0.051 and 1.490 ± 0.078 for 0.44 µm. The values of these indices are consistent

with the results obtained by [23, 24]. The values of the imaginary part vary from $(13.0 \pm 20.0).10^{-3}$ to $(157.6 \pm 172.1).10^{-3}$ at 0.44 µm, indicating a high absorption observed at the Birdsville site where size distributions are almost constant.

Table 5: Annual means of the real and imaginary part for refractive index (0.44µm)

Localization	Real part	Imaginairy part×10^{-3}	References (*)AERONET
Oujda, Maroc	1.490 ± 0.078	35.2 ± 39.0	(*) Diouri et al, 2015
Ouarzazate, Maroc	1.510 ± 0.053	86.7 ± 86.2	(*) E. Cuevas-Agullo et al, 2015
Tamanrasset, Algérie	1.484 ± 0.043	13.0 ± 20.0	(*) E. Cuevas-Agullo et al, 2015
Birdsville, Australie	1.564 ± 0.037	157.6 ± 17.2	(*) Ross-Mitchell, 2015
Dalanzadgad, Mongolie	1.560 ± 0.041	23.2 ± 22.9	(*) B Holben, 2014
Frenchman-Flat, Nevada	1.483 ± 0.051	17.9 ± 19.4	(*) Carol J Bruegge, 2013

Conclusion

The desert aerosol characterized by its optical parameters, which are relatively different according to their origin, in the case of refractive indices. The different Angstrom coefficients and asymmetry parameters have a relatively spatiotemporal regularity with values that are quite consistent with the particle distributions in two modes around 0.14 µm for the fine particles and 2.06 µm for the coarse ones. The general analysis of the different optical parameters of the different studied sites confirms the dominance of the Saharan zone. This is the main area with the greatest impact on both the radiative budget (large variation in radiative forcing) and the high concentrations, in mean, in the Sahara and its vicinity.

References

1. A.Tahiri. *Editions Universitaires Européennes* (2017). Thèse de Doctorat, ISBN 978-3-330-86848-9.
2. K. Kandler, L. Schütz, C. Deutscher, M. Ebert, H. Hofmann, S. Jäckel, R. Jaenicke, P. Knippertz, K. Lieke, A. Massling, A. Petzold, A. Schladitz, B. Weinzierl, A. Wiedensohler, S. Zorn, S. Weinbruch. *Tellus B* 61(1) (2009) 32-50. 12, 54, 57, 58.
3. K.O. Ogunjobi, Z. He, C. Simmer. *Atmospheric Research*, 88 (2008) 89-107.
4. H. D. Kambezidis and D. G. Kaskaoutis. *Atmospheric Environ*ment, 42 (2008) 1892-1906.
5. Y. Balkanski, M. Schulz, T. Claquin and S. Guibert. *Atmospheric Chemistry and Physics*, 7 (2006) 81-95. Doi: 10.5194/acp-7-81-2007.
6. A. Petzold, K. Rasp, B. Weinzierl, M. Esselborn, T. Hamburger, A. Dörnbrack, K. Kandler, L. Schütz, P. Knippertz, M. Fiebig, A. Virkkula. *Tellus B* (2009), Volume 61, Issue 1, February 2009, pages 118-130. Doi: 10.1111/j.1600-0889.2008.00383.x.
7. S. Otto, E. Bierwirth, B. Weinzierl, K. Kandler, M. Esselborn, M. Tesche, A. Schladitz, M. Wendisch, T. Trautmann. *Tellus B*, 61, Issue 1, (2009) 270-296. DOI: 10.1111/j.1600-0889.2008.00389.x.
8. A. Angstrom. *Geografiska Annaler*, 11(1929): 156-166.
9. B. N. Holben, D. Tanre, A. Smirnov, T. F. Eck, I. Slutsker, N. Abuhassen, W. W. Newcomb, J. Schafer, B. Chatenet, F. Lavenue, Y. J. Kaufman, J. Vande Castle, A. Setzer, B. Markham, D. Clark, R. Frouin, R. Halthore, A. Karnieli, N. T. O'Neill, C. Pietras, R. T. Pinker, K. Voss, G. Zibordi. *Journal of Geophysical Research-Atmospheres.* 106, No. D11 (2001) 12067-12097.
10. L. El Amraoui, M. Diouri, M. El Hitmy, R. Jaenicke, L. Schutz and W.von Hoyningen-Huene. *Journal Aerosol Science*. Vol 31 Supp 1 (2000) S 277- S278.
11. L. El Amraoui and M. Diouri. *Journal Aerosol Science*. 32 Supp 1 (2000) S643-S644.
12. A. Tahiri. Caractérisation de l'aérosol désertique, application au cas du Maroc (2015). *Thèse de Doctorat*, Université Mohamed Premier. Oujda, Maroc.

13. L. El Amraoui. Caractérisation optique de l'aérosol atmosphérique du nord du Maroc oriental (2001). *Thèse de Doctorat*, Université Mohamed Premier. Oujda, Maroc.
14. I. El Aouadi. Estimation de la quantité de vapeur d'eau précipitable et du forçage radiatif de l'aérosol atmosphérique à partir de la télédétection passive à Oujda (2005). *Thèse de Doctorat*, Université Mohamed Premier. Oujda, Maroc.
15. O. Dubovik, A. Sinyuk, T. Lapyonok, B. N. Holben, M. Mishchenko, P. Yang, T. F. Eck, H. Volten, O. Muñoz, B. Veihelmann, W. J. van der Zande, Jean-Francois Leon, M. Sorokin, I. Slutsker. *Journal of Geophysical Research Atmospheres*. 111, Issue D11 (2006). DOI: 10.1029/2005JD006619.
16. J. H. Seinfeld and S. N. Pandis. *Atmospheric Chemistry and Physics*. Wiley-Interscience Publication, Hoboken, ISBN: 978-1-118-94740-1, (1998).
17. Y. Fouquart, B. Bonnel, G. Brogniez, J. C. Buriez, L. Smith, J. J. Morcrette, A. Cerf. Observations of Saharan Aerosols: Results of ECLATS Field Experiment. Part II: Broadband Radiative Characteristics of the Aerosols and Vertical Radiative Flux Divergence. *J. Appl Meteor Climatol*, 26 (1987) 38-52.
18. G. A. D'Almeida, P. Koepke, and E. P. Shettle (1991). *Atmospheric Aerosols.* A. Deepak, 561 pp.
19. M. Hess, P. Koepke and I. Schult. *Bulletin of the American Meteorological Society*. 79(5) (1998) 831-844, 24, 32, 57, 62.
20. T. Müller, A. Schladitz, A. Massling, N. Kaaden, K. Kandler, A. Wiedensohler. *Tellus B,* 61, Issue 1, (2009) 79-95. Doi**:** 10.1111/j.1600-0889.2008.00399.x.
21. K. Kandler, K. Lieke, N. Benker, C. Emmel, M. Küpper, D. Müller-Ebert, M. Ebert, D. Scheuvens, A. Schladitz, L. Schütz, S. Weinbruch. *Tellus B.* 63, Issue 4 (2011) 475-496. Doi: 10.1111/j.1600-0889.2011.00550.x.
22. B.Weinzierl, D. Sauer, M. Esselborn, A. Petzold, A. Veira, M. Rose, S. Mund, M. Wirth, A. Ansmann, M. Tesche, S. Gross, V. Freudenthaler. *Tellus B,* 63, Issue 4 (2011) 589-618.
23. Y. Balkanski, M. Schulz, T. Claquin, S. Guibert. *Atmospheric Chemistry and physics*, 7 (2006) 81-95. DOI: 10.5194/acp-7-81-2007.
24. J. Haywood and O. Boucher. review, *Reviews of Geophysics*. 38(4) (2000) 513-543. Doi: 10.1029/1999 RG000078, 2000.

(2018); http://www.jmaterenvironsci.com